

Simulation of Three Dimensional Electrostatic Field Configuration in Wire Chambers : A Novel Approach

N. Majumdar ^{*}, S. Mukhopadhyay

*Nuclear Science Group, Saha Institute of Nuclear Physics, 1/AF Bidhannagar,
Kolkata - 700064, India*

Abstract

Three dimensional field configuration has been simulated for a simple wire chamber consisting of one anode wire stretched along the axis of a grounded square cathode tube by solving numerically the boundary integral equation of the first kind. A closed form expression of potential due to charge distributed over flat rectangular surface has been invoked in the solver using Green's function formalism leading to a nearly exact computation of electrostatic field. The three dimensional solver has been employed to study the effect of several geometrical attributes such as the aspect ratio ($\lambda = \frac{l}{d}$, defined as the ratio of the length l of the tube to its width d) and the wire modelling on the field configuration. Detailed calculation has revealed that the field values deviate from the analytic estimates significantly when the λ is reduced to 2 or below. Although the deviation is more towards the cathode surface in general, a noticeable departure is observed very close to the anode wire. The estimate of the electrostatic field at a close proximity of $1\mu m$ to the wire yields a remarkable deviation from the analytic values. The relative deviation of the present calculations from the analytic solution is more when the wire is modeled as a polygon while it becomes negligible in case of thin-wire approximation ($a \ll r$), a being the radius of the wire and r the distance of the observation point.

Key words: Boundary element method, Green's function, electrostatic field configuration, wire chamber

PACS: 02.70.Pt, 29.40.Cs

^{*} Corresponding author., Fax : 91 33 23374637

Email address: nayana.majumdar@saha.ac.in (N. Majumdar).

1 Introduction

Wire chambers are peerless tracking devices employed wherever it is necessary to detect and localize radiation. Starting from its application in nuclear and subnuclear physics, it has been employed in widely different fields such as biology, medicine, space, industrial radiology, over last three decades or more. The normal operation of a wire chamber is based on the collection of the charges created by direct ionization of the gas medium by the passage of radiation. The charges are collected on the electrodes by application of an electric field across the chamber. From the electric pulses, thus generated, the relevant information regarding the radiation is extracted. The flexibility in the design of wire chambers allows for highly innovative and often considerably complex ones necessitating meticulous investigations on their structure and performance. The study of the electrostatic field plays a key role in optimizing the design of these state of the art detectors to get a desired configuration for the field in a given volume as per the tracking requirement. The analytic solution of the field configuration for a specific geometry is always the best choice to do the same. However, the analytic solution can be derived for severely restricted geometries which is often not applicable to realistic and complicated wire chambers [1,2]. The diversity in the chamber design necessitates application of other techniques for numerical estimation like Finite Element Method (FEM) and Finite Difference Method (FDM) [3,4]. FEM is more widely used for the reason that it can seamlessly handle any arbitrary geometry including even dielectrics. However, FEM has several drawbacks as well. It computes only the potential from which the electrostatic field can be obtained through numerical differentiation. The field values thus calculated, are unacceptable in the regions where the field gradient changes rapidly. Moreover, the interpolation of potential at the non-nodal points reduces accuracy significantly. The other approach which can yield nominally exact result is Boundary Integral Equation (BIE) method. This method is less popular due to its complicated mathematics and inaccuracies near the boundaries. However, for the present problem of computation of electrostatic field in wire chambers, BIE method is reasonably more suitable. It can provide accurate estimate of the electrostatic field at any arbitrary point by employing Green's function formulation which is necessary to study the avalanche happening anywhere in the chamber due to the passage of radiation. A brief comparison of BEM, the numerical implementation of BIE method, with FEM and FDM in the context of calculating three dimensional field configuration in wire chambers has been presented in [5].

The major drawback of BEM is related to the approximations involved in its numerical implementation. The approximations give rise to the infamous numerical boundary layer where the method suffers from gross inaccuracies [6]. This may lead to inaccurate estimation of electrostatic field configuration

which is not desirable in the close vicinity of the wires or the cathode. Recently, we have made a novel approach in the formulation of BEM using analytic expressions for potential and electrostatic field which leads to their nominally exact evaluation. The analytic expressions being valid throughout the physical volume, the formulation is capable of yielding accurate values even in the near-field region. The application of this Nearly Exact Boundary Element Method (NEBEM) solver [7] for the estimation of electrostatic field in a wire chamber of elementary geometry and the new results have been presented in this paper.

2 Present Approach

For electrostatic problems, the BIE can be expressed as

$$\phi(\vec{r}) = \int_S G(\vec{r}, \vec{r}') \rho(\vec{r}') dS' \quad (1)$$

where $\phi(\vec{r})$ represents potential at \vec{r} integrating the integrand over boundary surface S , $\rho(\vec{r}')$ the charge density at \vec{r}' and $G(\vec{r}, \vec{r}') = 1/4\pi\epsilon|\vec{r} - \vec{r}'|$ with ϵ being the permittivity of the medium. The BIE is numerically solved by discretizing the charge carrying surface S in a number of segments on which uniform charge densities ρ are assumed to be distributed. The discretization leads to a matrix representation of the BIE as follows

$$\mathbf{A} \cdot \rho = \phi \quad (2)$$

where A_{ij} of \mathbf{A} represents the potential at the mid-point of segment i due to a unit charge density distribution at the segment j . For known potential ϕ , the unknown charge distribution ρ is estimated by solving Eqn.(2) with the elements of influence matrix \mathbf{A} modeled by a sum of known basis functions with constant unknown coefficients.

In the present approach, namely NEBEM, the influences are calculated using analytic solution of potential and electrostatic field due to a uniform charge distribution over a flat rectangular surface. The expression for the potential ϕ at a point $P(X, Y, Z)$ in free space due to uniform unit charge density distributed on a rectangular surface having corners at $(x_1, 0, z_1)$ and $(x_2, 0, z_2)$ as shown in Fig.1 can be represented as a multiple of

$$\phi(X, Y, Z) = \int_{z_1}^{z_2} \int_{x_1}^{x_2} \frac{dx dz}{\sqrt{(X - x)^2 + Y^2 + (Z - z)^2}} \quad (3)$$

where the multiple depends upon the strength of the source and other physical considerations. The closed form expression for $\phi(X, Y, Z)$ can be deduced from the Eqn.(3). This can be expressed as follows.

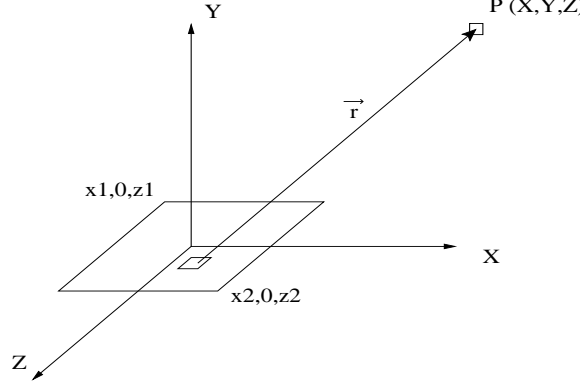


Fig. 1. A rectangular surface with uniform distributed source

$$\begin{aligned}
\phi(X, Y, Z) = & \\
& (X - x_1) \ln \left(\frac{D_{12} - (Z - z_2)}{D_{11} - (Z - z_1)} \right) + (X - x_2) \ln \left(\frac{D_{21} - (Z - z_1)}{D_{22} - (Z - z_2)} \right) \\
& + (Z - z_1) \ln \left(\frac{D_{21} - (X - x_2)}{D_{11} - (X - x_1)} \right) + (Z - z_2) \ln \left(\frac{D_{12} - (X - x_1)}{D_{22} - (X - x_2)} \right) \\
& + \frac{i |Y|}{2} \\
& (S_1 (\tanh^{-1} \left(\frac{R_1 + i I_1}{D_{11} |Z - z_1|} \right) - \tanh^{-1} \left(\frac{R_1 - i I_1}{D_{11} |Z - z_1|} \right) \\
& + \tanh^{-1} \left(\frac{R_1 - i I_2}{D_{21} |Z - z_1|} \right) - \tanh^{-1} \left(\frac{R_1 + i I_2}{D_{21} |Z - z_1|} \right)) \\
& + S_2 (\tanh^{-1} \left(\frac{R_2 + i I_2}{D_{22} |Z - z_2|} \right) - \tanh^{-1} \left(\frac{R_2 - i I_2}{D_{22} |Z - z_2|} \right) \\
& + \tanh^{-1} \left(\frac{R_2 + i I_1}{D_{12} |Z - z_2|} \right) - \tanh^{-1} \left(\frac{R_2 - i I_1}{D_{12} |Z - z_2|} \right))) \\
& - 2\pi Y
\end{aligned} \tag{4}$$

where

$$\begin{aligned}
D_{11} &= \sqrt{(X - x_1)^2 + Y^2 + (Z - z_1)^2}; D_{12} = \sqrt{(X - x_1)^2 + Y^2 + (Z - z_2)^2} \\
D_{21} &= \sqrt{(X - x_2)^2 + Y^2 + (Z - z_1)^2}; D_{22} = \sqrt{(X - x_2)^2 + Y^2 + (Z - z_2)^2} \\
R_1 &= Y^2 + (Z - z_1)^2; R_2 = Y^2 + (Z - z_2)^2 \\
I_1 &= (X - x_1) |Y|; I_2 = (X - x_2) |Y|; S_1 = \text{sign}(z_1 - Z); S_2 = \text{sign}(z_2 - Z)
\end{aligned}$$

The electrostatic field can similarly be represented as a multiple of

$$\vec{F}(X, Y, Z) = \int_{z_1}^{z_2} \int_{x_1}^{x_2} \frac{\hat{r} dx dz}{r^2} \quad (5)$$

where \vec{r} is the displacement vector from an element to the point (X, Y, Z) where the field will be evaluated. The integration of Eqn. (5) gives the exact expressions for the field in X , Y and Z -directions as follow.

$$F_x(X, Y, Z) = \ln \left(\frac{D_{11} - (Z - z_1)}{D_{12} - (Z - z_2)} \right) + \ln \left(\frac{D_{22} - (Z - z_2)}{D_{21} - (Z - z_1)} \right) \quad (6)$$

$$\begin{aligned} F_y(X, Y, Z) = & \\ & -\frac{i}{2} \text{Sign}(Y) \\ & (S_1 (\tanh^{-1} \left(\frac{R_1 + i I_1}{D_{11} |Z - z_1|} \right) - \tanh^{-1} \left(\frac{R_1 - i I_1}{D_{11} |Z - z_1|} \right) \\ & + \tanh^{-1} \left(\frac{R_1 - i I_2}{D_{21} |Z - z_1|} \right) - \tanh^{-1} \left(\frac{R_1 + i I_2}{D_{21} |Z - z_1|} \right)) \\ & + S_2 (\tanh^{-1} \left(\frac{R_2 + i I_2}{D_{22} |Z - z_2|} \right) - \tanh^{-1} \left(\frac{R_2 - i I_2}{D_{22} |Z - z_2|} \right) \\ & + \tanh^{-1} \left(\frac{R_2 + i I_1}{D_{12} |Z - z_2|} \right) - \tanh^{-1} \left(\frac{R_2 - i I_1}{D_{12} |Z - z_2|} \right)) \\ & + C \end{aligned} \quad (7)$$

$$F_z(X, Y, Z) = \ln \left(\frac{D_{11} - (X - x_1)}{D_{21} - (X - x_2)} \right) + \ln \left(\frac{D_{22} - (X - x_2)}{D_{12} - (X - x_1)} \right) \quad (8)$$

In Eqn.(7), C is a constant of integration as follows:

$$C = \begin{cases} 0 & \text{if outside the extent of the flat surface} \\ 2\pi & \text{if inside the extent of the surface and } Y > 0 \\ -2\pi & \text{if inside the extent of the surface and } Y < 0 \end{cases}$$

All these equations have been used as foundation of the three dimensional solver [8].

In the present problem, two different modelling schemes of the wire have been used to study the field configuration. When the wire has been modeled as

a polygon, the above expressions from Eqn.(4)- Eqn.(8) have been employed to estimate the potential and the electrostatic field. In the other model, the wire has been considered as a thin wire where the radius of the wire a has been assumed to be small compared to the distance r of the observation point ($a \ll r$). The expression for the potential at any point due to a wire element along Z -axis is the following.

$$\phi(X, Y, Z) = 2\pi a \log \left(\frac{\sqrt{X^2 + Y^2 + (h+Z)^2} + (h+Z)}{\sqrt{X^2 + Y^2 + (h-Z)^2} - (h-Z)} \right) \quad (9)$$

where h is the half of the length of the wire element. It should be mentioned here that the analytic solution of the two dimensional electrostatic field of a doubly periodic wire array in the Garfield code [9] is derived using a similar thin-wire approximation [1]. The expressions for the electrostatic field components can be presented as the following under the same assumption.

$$F_x(X, Y, Z) = 2\pi a X \left(\frac{(h-Z)\sqrt{X^2 + Y^2 + (h+Z)^2} + (h+Z)\sqrt{X^2 + Y^2 + (h-Z)^2}}{(X^2 + Y^2)\sqrt{X^2 + Y^2 + (h-Z)^2}\sqrt{X^2 + Y^2 + (h+Z)^2}} \right) \quad (10)$$

$$F_y(X, Y, Z) = 2\pi a Y \left(\frac{(h-Z)\sqrt{X^2 + Y^2 + (h+Z)^2} + (h+Z)\sqrt{X^2 + Y^2 + (h-Z)^2}}{(X^2 + Y^2)\sqrt{X^2 + Y^2 + (h-Z)^2}\sqrt{X^2 + Y^2 + (h+Z)^2}} \right) \quad (11)$$

$$F_z(X, Y, Z) = 2\pi a \left(\frac{\sqrt{X^2 + Y^2 + (h+Z)^2} - \sqrt{X^2 + Y^2 + (h-Z)^2}}{\sqrt{X^2 + Y^2 + (h+Z)^2}\sqrt{X^2 + Y^2 + (h-Z)^2}} \right) \quad (12)$$

However, a separate set of expressions is needed to evaluate the potential and electrostatic field due to a wire element along its axis. These incorporate the effect of finite radius of the wire element and are expressed below.

$$\phi(0, 0, Z) = 2\pi a \log \left(\frac{\sqrt{a^2 + (h+Z)^2} + (h+Z)}{\sqrt{a^2 + (h-Z)^2} - (h-Z)} \right) \quad (13)$$

In this case, only the Z -component of the field is non-zero and can be written as

$$F_z(0, 0, Z) = 2\pi a \left(\frac{\left(\sqrt{(h+Z)^2 + a^2} - \sqrt{(h-Z)^2 + a^2} \right)}{\sqrt{(h-Z)^2 + a^2}\sqrt{(h+Z)^2 + a^2}} \right) \quad (14)$$

3 Numerical Implementation

The present problem studied with the NEBEM is to compute the electrostatic potential and field for a simple geometry consisting of a single anode wire running along the axis of a square tube. A schematic diagram of the wire chamber has been illustrated in Fig.2. The anode wire has been supplied a positive high voltage of 1000 Volt and the surrounding cathode tube is grounded. Several

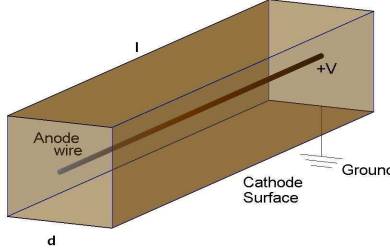


Fig. 2. Schematic representation of the wire chamber. The length and the width of the square tube are represented by l and d respectively. The anode wire along its axis has diameter $2a$. The wire is supplied a voltage $+V$ and the cathode is kept grounded.

cases for altered tube cross section ($d \times d$), length (l), wire diameter ($2a$) as well as wire modelling have been studied. The four flat rectangular surfaces in this chamber have been segmented in to 21×21 elements. The wire when considered as a polygon has been modeled with 12 surfaces each divided in 21 axial rectangular segments. The maximum number of elements in the influence matrix has become 2016 with polygon representation while it has reduced to 1785 for thin-wire representation. The maximum user time has reached approximately ten minutes on a Pentium IV machine with 2GB RAM running Fedora Core 3. It should be noted here that if only the mid-plane estimates of the wire chamber are of importance, the computation time can be reduced drastically by using even one element in the axial direction resulting into less than 100 slender elements in total for the present problem.

4 Results

The NEBEM calculations for potential and normal electrostatic field (Y -component) at the mid-plane of the chamber have been compared with the analytic estimates of an infinitely long tube provided by the Garfield code [9] to demonstrate the accuracy of the solver. In Fig.3 and Fig.4, the re-

sults are shown for a variation in the tube cross-section from $5mm \times 5mm$ to $16mm \times 16mm$ with wire diameter $50\mu m$, the wire being modeled as a polygon. The aspect ratio, $\lambda = \frac{l}{d}$, has been kept 10 to retain the property of infiniteness so as to compare with analytic estimates of an infinitely long tube. The comparison shows an excellent agreement over the whole range of tube dimensions. In Fig.4, the field values have been calculated at a spatial

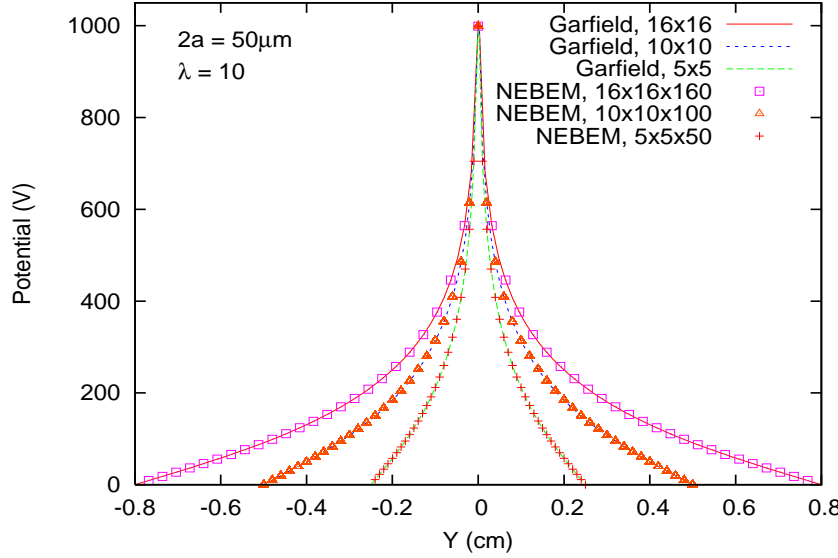


Fig. 3. Comparison of potential at the mid-plane of the chamber with aspect ratio 10 and wire diameter $50\mu m$. Three variations in the chamber cross-section are illustrated along with analytic values.

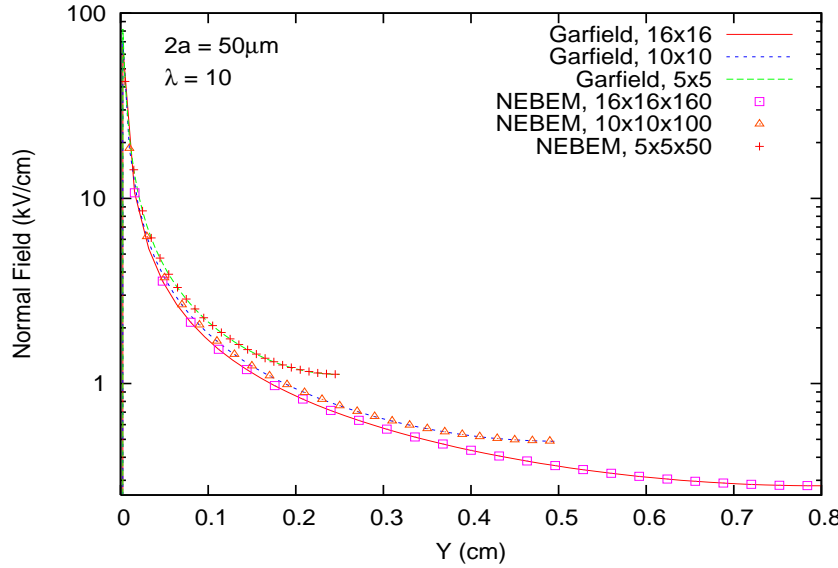


Fig. 4. Comparison of normal electric field at the mid-plane of the chamber with aspect ratio 10 and wire diameter $50\mu m$. Three cases of varied cross-sections are illustrated along with analytic estimates.

frequency of $100\mu\text{m}$ using the polygon model for the anode wire. The values computed throughout the cross-section of the tube by the NEBEM agree excellently with the analytic calculation except at very close vicinity to the anode wire which will be discussed later.

The NEBEM is a full-fledged three dimensional solver and hence the effect of λ of the tube on the field configuration can be studied using it. From several such studies it has been observed that the departure from the analytic solutions for an infinitely long tube becomes significant when λ is reduced to 2 and below. This has been illustrated in Fig.5 by plotting the relative deviation of normal electrostatic field between the analytic and the NEBEM calculations, defined as

$$\text{Error}(\%) = \frac{\text{Garfield} - \text{NEBEM}}{\text{Garfield}} \times 100 \quad (15)$$

The calculation has been done for the mid-plane of the tube for a wide variation in λ . The cross-section of the tube has been considered to be $10\text{mm} \times 10\text{mm}$ with wire diameter $50\mu\text{m}$ modeled as both polygon and a thin wire. It has been seen that with the polygon model, the relative deviation towards

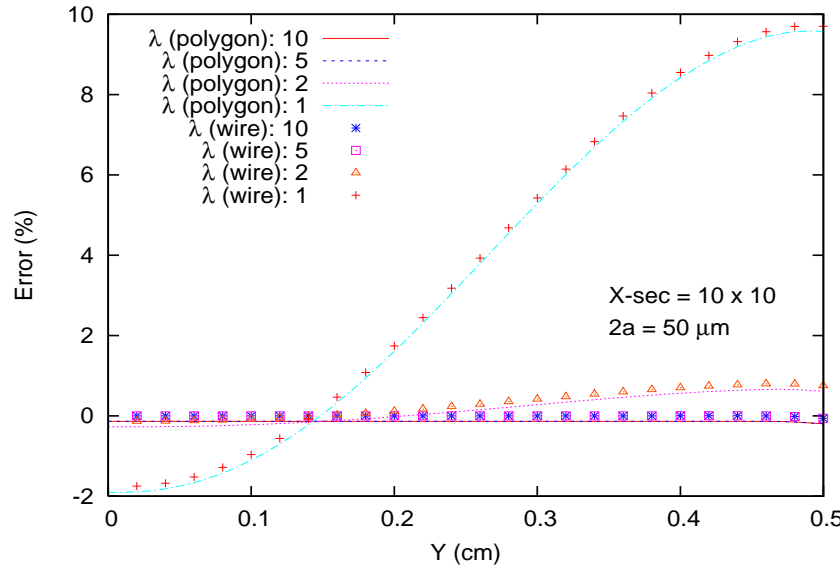


Fig. 5. Relative deviation of normal electric field from the analytic values at the mid-plane of the chamber with varied aspect ratios for polygon and thin-wire modelling of the wire. The cross-section of the chamber and the diameter of the wire are $10\text{mm} \times 10\text{mm}$ and $50\mu\text{m}$ respectively.

the cathode or the body of the tube becomes apparent (close to 1%) as λ is dropped down to 2. It enhances up to 10% near the cathode surface while more than 2% near the anode wire when λ is still reduced to 1. The results obtained with thin-wire approximation agree with the analytic values with the relative

deviation being less than 0.05% towards the cathode and even less near the anode at larger λ s. The effect of reduction in λ is similar to that observed in the polygon model.

Since NEBEM can evaluate three dimensional field at any point in the physical volume including the near-field region, a study has been carried out to calculate the field values at a close proximity of $1\mu m$ only to the anode wire. A significant difference has been noticed between the present results and the analytic values. Although this has been illustrated in Fig.4, it is not clearly visible in the figure. In order to facilitate this comparison, the present results have been presented numerically in Table 1 which contains the field values for a tube with $\lambda = 10$. As is evident from the values, the NEBEM results at $1\mu m$ away from the anode wire are significantly lower than the analytic results. The latter can be reproduced when the wire is represented by a thin-wire model for obvious reason. It should be noted from the Table 1 that the relative deviation

Table 1

Comparison of normal field values with polygon and wire modelling of the wire of diameter $50\mu m$. The aspect ratio of the chamber is 10.

Cross-section (mm \times mm)	Garfield (kV/cm)	NEBEM (polygon) (kV/cm)	NEBEM (wire) (kV/cm)
16 \times 16	6.5813e+01	4.924316e+01	6.581150e+01
10 \times 10	7.1569e+01	5.355572e+01	7.156708e+01
5 \times 5	8.2166e+01	6.149857e+01	8.216439e+01

at $1\mu m$ away from the anode wire is as large as 25% with the polygon model while for a thin-wire model of the wire, the relative deviation is only 0.003%. The reduction in λ down to 1 reduces the former to 23%. It has been noted that even with the thin-wire representation which can reproduce the analytic estimates for all cases presented above, the drop in λ to 1 makes the deviation as large as 18%.

Finally, the variation of normal electrostatic field along the axial direction of the tube has been studied which has been plotted in Fig.6. The tube dimension has been considered to be $10mm \times 10mm \times 100mm$ with wire diameter $50\mu m$. The calculations have been carried out at three different transverse locations as indicated in the figure. The middle line represents the calculation done at halfway between the anode and the cathode. The two dimensional analytic solutions provided by the Garfield code have been illustrated in three dimension by the lines representing the uniform field configuration throughout the length. The NEBEM results reproduce the two dimensional analytic values for more than 85% of the tube length. However, in the remaining 15% towards the ends, the three dimensional effects are non-negligible. Even more important point to be noted here is that the NEBEM calculation produces

perfectly smooth variation of the field with a spatial frequency of $10\mu\text{m}$ only while significant fluctuations are known to be present in FDM, FEM and usual BEM solvers because of their strong dependence on nodal properties. This remarkable feature of the present solver should allow more realistic estimation of the electrostatic field of various gas detectors resulting into better gain estimations.

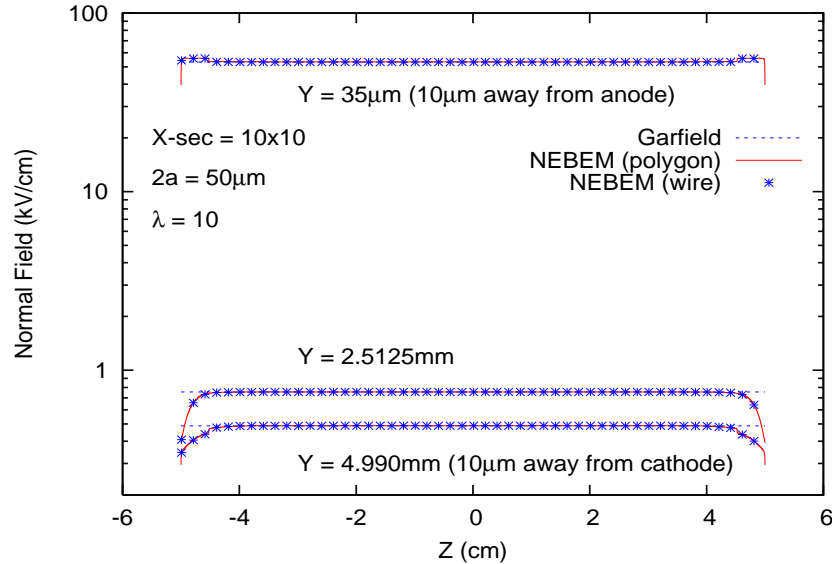


Fig. 6. Axial deviation of normal electric field at the mid-plane of the chamber with cross-section $10\text{mm} \times 10\text{mm}$, aspect ratio 10 and wire diameter $50\mu\text{m}$, calculated at three Y -positions. Two different wire models are considered.

5 Conclusion

The three dimensional NEBEM solver has yielded several significant observations in the electrostatic field configuration of a wire chamber of elementary geometry. It has been found that the modelling of the anode wire plays an important role in the field configuration which leads to a departure of about 25% from the analytic estimate at a very close proximity of $1\mu\text{m}$ near the anode wire which is within the region of prime importance in the study of avalanche in wire chambers. The disagreement can be accounted for with the thin-wire approximation as expected since the same approximation is used in the analytic calculations. The NEBEM solver has also exhibited the effect of finite geometry on the field configuration. The field values even at the mid-plane of the chamber start to show a departure from the analytic ones calculated for infinitely long chamber when λ of the chamber is reduced to 2 and below. Even the thin-wire approximation can not reduce the deviation below 18% when λ is made 1. The simple but robust formulation of the solver using closed form

expressions can also be used to solve for wire chambers of other geometries. Since the solver can produce very smooth and precise estimate of three dimensional electrostatic field even in the near-field region, it should be very useful in providing important information related to the design and interpretation aspects of a wire chamber.

6 Acknowledgement

The authors are thankful to Prof. B. Sinha, Director, SINP, and Prof. S. Bhattacharya, Head, NAP Division of SINP for their encouragement and support throughout this work.

References

- [1] G. A. Erskine, *Nuclear Instrumentation and Methods* **105** (1972) 565.
- [2] R. Veenhof, *Nuclear Instruments and Methods in Physics Research A* **419** (1998) 726.
- [3] W. I. Buchanan and N. K. Gupta, *Advances in Engineering Software* **23** (1995) 111.
- [4] T. M. Lopez and A. Sharma, *CERN/IT/99/5* **7** (1997).
- [5] S. Mukhopadhyay and N. Majumdar, *IEEE Transactions on Nuclear Science* **53**, No.2 (2006) (to be published)
- [6] A. Renau, F. H. Read and J. N. H. Brunt, *Journal of Physics E: Science Instruments* **15** (1982) 347.
- [7] S. Mukhopadhyay and N. Majumdar, *Advances in Computational and Experimental Engineering and Sciences* TechScience Press, 2005
- [8] S. Mukhopadhyay and N. Majumdar, *Engineering Analysis with Boundary Elements* (accepted)
- [9] <http://garfield.web.cern.ch/garfield>